

Electronic and phononic Raman scattering in detwinned $\text{YBa}_2\text{Cu}_3\text{O}_{6.95}$ and $\text{Y}_{0.85}\text{Ca}_{0.15}\text{Ba}_2\text{Cu}_3\text{O}_{6.95}$: s -wave admixture to the $d_{x^2-y^2}$ -wave order parameter

M. Bakr,¹ A. P. Schnyder,² L. Klam,¹ D. Manske,¹ C.T. Lin,¹ B. Keimer,¹ M. Cardona,¹ and C. Ulrich¹

¹Max-Planck-Institut für Festkörperforschung, Heisenbergstr. 1, D-70569 Stuttgart, Germany

²Kavli Institute for Theoretical Physics, University of California, Santa Barbara, CA 93106, USA

(Dated: October 29, 2018)

Inelastic light (Raman) scattering has been used to study electronic excitations and phonon anomalies in detwinned, slightly overdoped $\text{YBa}_2\text{Cu}_3\text{O}_{6.95}$ and moderately overdoped $\text{Y}_{0.85}\text{Ca}_{0.15}\text{Ba}_2\text{Cu}_3\text{O}_{6.95}$ single crystals. In both samples modifications of the electronic pair-breaking peaks when interchanging the a - and b -axis were observed. The lineshapes of several phonon modes involving plane and apical oxygen vibrations exhibit pronounced anisotropies with respect to the incident and scattered light field configurations. Based on a theoretical model that takes both electronic and phononic contributions to the Raman spectra into account, we attribute the anisotropy of the superconductivity-induced changes in the phonon lineshapes to a small s -wave admixture to the $d_{x^2-y^2}$ pair wave-function. Our theory allows us to disentangle the electronic Raman signal from the phononic part and to identify corresponding interference terms. We argue that the Raman spectra are consistent with an s -wave admixture with an upper limit of 20 percent.

PACS numbers: 74.20.Rp, 74.25.Gz, 74.25.Kc, 74.72.Bk

I. INTRODUCTION

The symmetry of the pair wavefunction provides important clues to the mechanism of high temperature superconductivity. Phase sensitive experiments have shown that the dominant component of the order parameter exhibits $d_{x^2-y^2}$ symmetry.^{1,2} In cuprates of the $\text{YBa}_2\text{Cu}_3\text{O}_{7-\delta}$ -type with orthorhombic crystal symmetry, an s -wave admixture resulting in an anisotropy of the superconducting (SC) energy gap, 2Δ , between the a - and b -axes is expected. A more general trend of increasing s -wave admixture with increasing doping level has also been reported.^{3,4,5,6} In $\text{YBa}_2\text{Cu}_3\text{O}_{7-\delta}$ (YBCO_{7- δ}), such an admixture has been confirmed by angle-resolved photoemission spectroscopy (ARPES)⁷ and flux measurements on Josephson junctions.⁸ However, the interpretation of the ARPES data is complicated because the surface properties of YBCO_{7- δ} may differ from those of the bulk.⁹ The phase-sensitive measurements, on the other hand, have yielded only lower bounds (9%) to the s -wave admixture. In addition, phenomenological calculations based on the two-dimensional Hubbard model^{10,11} have demonstrated that the in-plane anisotropy of the spin fluctuation spectrum determined by inelastic neutron scattering on detwinned YBCO^{12,13} is consistent with a small isotropic s -wave admixture to the $d_{x^2-y^2}$ -pairing symmetry. However, the same calculations show that the dispersion and spectral weight of the spin fluctuations are also influenced by anisotropic hopping parameters that are difficult to determine independently. Moreover, different interpretations of the neutron data have also been proposed^{14,15}. Further experiments are therefore required to conclusively establish the magnitude of the s -wave contribution to the SC gap in YBCO_{7- δ} .

Inelastic light (Raman) scattering is a powerful probe of electronic and lattice vibrational excitations in high- T_c superconductors.^{16,17} Both electronic and phononic Raman scattering have been applied to study the superconducting gap anisotropy in YBCO_{7- δ} . The anisotropy can be inferred

from the energies of gap features of the electronic continuum in various polarization geometries,^{6,18} but the accuracy of this method is limited by overlap with Raman-active phonons. Possible manifestations of the gap anisotropy and an anisotropic electron-phonon coupling in the lineshape of a Raman-active out-of-plane vibration of the in-plane oxygen atoms of B_{1g} symmetry have also been investigated.¹⁹ However, the analysis of these data has been contested,²⁰ and a quantitative estimate of the gap anisotropy has not been extracted from them.

The present work was in part motivated by a recent theoretical study that yielded quantitative predictions for the electronic Raman continua in a $(d_{x^2-y^2} + s)$ -wave superconductor.²¹ In order to enable a detailed comparison with these predictions, we have performed Raman scattering measurements of the temperature dependence of the electronic continua and phonon modes in twin-free, slightly overdoped YBCO_{6.95} and moderately overdoped $\text{Y}_{0.85}\text{Ca}_{0.15}\text{Ba}_2\text{Cu}_3\text{O}_{6.95}$ (henceforth YBCO_{6.95:Ca}) single crystals. We found that interference between the electronic and phononic scattering channels imposed severe limitations on our capability to extract information about the gap anisotropy from the electronic continuum alone, in accordance with previous work.^{6,18} We have therefore employed a phenomenological model that treats the electronic and phononic contributions to the Raman signal on equal footing. This formalism yields predictions for the energy, intrinsic linewidth, and Fano parameters of phonons coupled to the electronic continuum as a function of temperature. From a comparison to the experimentally determined lineshapes of two phonon modes, the B_{1g} vibration of the in-plane oxygen at 340 cm^{-1} as well as an apical-oxygen vibration at 501 cm^{-1} , we extract an upper bound of 20% on the s -wave admixture to the SC energy gap. This is consistent with a 10% to 15% admixture of s -wave to the $d_{x^2-y^2}$ pair-breaking peak observed in the electronic continuum in the superconducting state, and it coincides with the lower bound extracted from the phase-sensitive measurements⁸. Similar effects have been recently reported for an organic superconductor with the

same point group as $\text{YBa}_2\text{Cu}_3\text{O}_{7-\delta}$ (D_{2h}). In this case, however, the analysis led to the conclusion that only an isotropic s -wave state is present.²²

This paper is organized as follows. In Sec. II we describe experimental details and discuss the raw Raman spectra. An introduction to our theoretical model is given in Sec. III. In particular, we focus on a simultaneous description of both, the electronic Raman response and the phonon anomalies above and below T_c . Based on this description we are able to analyze the superconductivity-induced changes in the phonon lineshape in Sec. IV. A summary of our results and a comparison to prior work is contained in Sec. V.

II. EXPERIMENTAL DETAILS

High quality single crystals of $\text{YBCO}_{6.95}$ and $\text{YBCO}_{6.95}:\text{Ca}$ were grown by the top-seeded solution growth method.²³ The orientations of the crystallographic axes were determined by Laue x-ray diffraction and polarized light microscopy. The samples were then cut into rectangular shapes of typical size $3 \times 3 \times 1 \text{ mm}^3$, annealed at 520°C in a flow of oxygen gas for 150 hours, and quenched in liquid nitrogen in order to avoid further oxygen diffusion. The magnetization curves of the $\text{YBCO}_{6.95}$ ($\text{YBCO}_{6.95}:\text{Ca}$) crystal show an onset of $T_c = 92 \text{ K}$ (75 K). A transition width ΔT_c of less than 3 K (6 K) indicates good homogeneity of the samples. Employing Tallon's phenomenological expression,²⁴ the hole doping level of our samples is estimated as 0.17 (0.21) per planar Cu ion, i.e., they are slightly (moderately) overdoped. The crystals were detwinned individually using the procedure described in Refs. 25 and 26. Raman spectra measured at different spots of the ab -surface of each sample look basically the same, thus confirming the homogeneity of our single crystals.

The Raman scattering experiments were performed in backscattering geometry using a Dilor XY-triple grating Raman spectrometer with a CCD camera as detector. For excitation, the 514.5 nm line of an Ar^+/Kr^+ mixed gas laser was used. The resolution of our spectrometers for this experiment was about 3 cm^{-1} . In order to avoid heating of the sample, the power of the incident laser was kept below 10 mW at the sample surface with a laser spot of $100 \mu\text{m}$ in diameter. The direction of the incident laser light was always parallel to the crystallographic c -axis. For the selection rule analysis, a polarizer and an analyzer were placed into the light path before and after the sample.

$\text{YBCO}_{6.95}$ and $\text{YBCO}_{6.95}:\text{Ca}$ are orthorhombic with the space group $Pmmm$ (D_{2h} symmetry). In polarized Raman scattering experiments, excitations of A_g , B_{1g} , A_g+B_{1g} , and A_g symmetries are accessible by using xx (or yy), xy (or yx), $x'x'$ (or $y'y'$), and $x'y'$ (or $y'x'$) polarizations of the incident and scattered light fields, respectively.^{17,27} In this notation x and y correspond to the direction of the electric field of light along the a - and b -axes, whereas x' and y' correspond to the diagonal directions, i.e. $x' \sim x + y$ and $y' \sim x - y$, respectively. As most previous work on YBCO has been performed on twinned specimens, we follow previous publica-

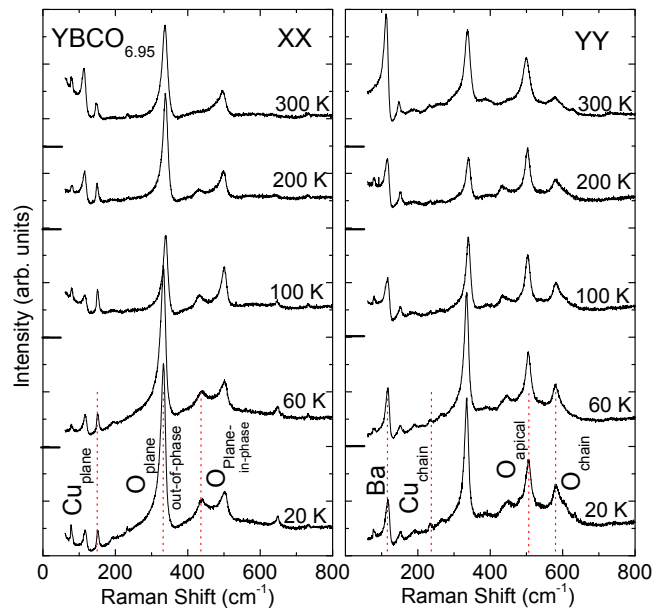


FIG. 1: Raman spectra of a detwinned slightly overdoped $\text{YBa}_2\text{Cu}_3\text{O}_{6.95}$ single crystal in xx and yy polarization taken with an Ar^+ laser line ($\lambda=514.5 \text{ nm}$). The mode assignment corresponds to Refs. 32,33,34,35,36. The spectra were shifted by a constant offset with respect to each other. The intensity scales in left and right panels are the same

tions and use the tetragonal notation of the polarization symmetries throughout this paper. In this notation, the structure is described in terms of the closely related tetragonal point group D_{4h} , and the excitations of A_g+B_{1g} symmetry are accessible for either xx or yy polarization, B_{2g} for either xy or yx polarization, A_g+B_{2g} for either $x'x'$ or $y'y'$ polarization, and B_{1g} for either $x'y'$ or $y'x'$ polarization of the incident and scattered electric field vectors.

Figure 1 show Raman spectra of detwinned $\text{YBCO}_{6.95}$ crystals measured at various temperatures. As in other high- T_c superconductors,^{16,28,29,30,31} the normal-state spectra exhibit a flat electronic continuum with superimposed phonons. Below T_c , a significant fraction of the electronic spectral weight is transferred to higher energies, resulting in a broad pair-breaking peak in the electronic continuum. In addition, the phonon lineshapes reveal characteristic changes. In B_{1g} polarization this spectral-weight redistribution is most pronounced because electronic Raman scattering in this geometry is sensitive to the maximum of the SC gap along the anti-nodal direction of the two-dimensional SC gap. We therefore focus in this work on this geometry, along with the xx and yy polarization channels that provide direct information about the in-plane anisotropy of the electronic response.

Figure 1 gives an overview of the phonon modes of $\text{YBCO}_{6.95}$ in the xx and yy polarization geometries. As expected based on a group-theoretical analysis,^{17,32,33,34,35,36} five phonons appear in both polarization channels. The lowest-frequency phonon at 113 cm^{-1} (A_{1g}) originates predominantly from vibrations of the barium atoms. The next low-

est frequency phonon at 148 cm^{-1} (A_{1g}) corresponds mainly to the vibrations of copper (Cu2 ions). The vibrations of the apical oxygen ions (O4) appears at 501 cm^{-1} (A_{1g}). The two modes at 340 cm^{-1} (B_{1g}) and 446 cm^{-1} (A_{1g}) originate from out-of-phase and in-phase vibrations of the planar oxygen ions (O2 and O3), respectively.³² Two additional defect-induced modes appear in the yy symmetry at 232 cm^{-1} and at 579 cm^{-1} . They originate from vibrations of the copper (Cu1) and the oxygen (O1) ions, respectively, in the Cu–O chains, which are aligned along the crystallographic b -axis.³⁵ In YBCO crystals with fully oxygenated chains, these two modes are Raman forbidden but infrared-allowed (B_{1u} symmetry).^{37,38,39} They become Raman-active due to breaking of the translational symmetry by defects, *i.e.*, unoccupied oxygen positions in the Cu1-O1 chains.^{33,34,35} The absence of the strong mode at 579 cm^{-1} in the data with xx polarization confirms the high detwinning ratio of our crystal ($\sim 95\%$).

III. ANALYSIS OF RAMAN SPECTRA

The measured Raman intensity $I_\sigma(\omega)$ in a given polarization channel σ is related to the imaginary part of the response function $\text{Im} \chi_\sigma(\omega)$ via $I_\sigma(\omega) = A [1 + n(\omega)] \text{Im} \chi_\sigma(\omega)$, where $n(\omega)$ denotes the Bose distribution and A is a coupling constant. The Raman response in cuprate superconductors in the optimally and overdoped regimes consists of electronic (intradband) and phononic excitations. In order to disentangle these two contributions it is necessary to employ a proper fitting procedure. A phonon interacting with intraband excitations acquires a renormalized self-energy and exhibits an asymmetric, Fano-type Raman lineshape. To describe such an electron-phonon coupled Raman spectrum the following formula can be employed^{40,41,42,43,44,45}

$$\text{Im} \chi_\sigma(\omega) = \rho_\sigma(\omega) + \frac{g_\sigma^2}{\Gamma(\omega) [1 + \epsilon^2(\omega)]} \times \{S^2(\omega) - 2\epsilon(\omega)S(\omega)\rho_\sigma(\omega) - \rho_\sigma^2(\omega)\}, \quad (1)$$

where $\epsilon(\omega) = (\omega^2 - \Omega^2)/2\omega_0\Gamma(\omega)$ and $S(\omega) = S_0 + R_\sigma(\omega)$. The renormalized phonon frequency and the renormalized phonon line width are given by $\Omega^2 = \omega_0^2 - 2\omega_0g_\sigma^2R_\sigma(\omega)$, and $\Gamma(\omega) = \Gamma_0 + g_\sigma^2\rho_\sigma(\omega)$, respectively, with the intrinsic phonon frequency ω_0 and the bare phonon line width Γ_0 . The parameter S_0 can be expressed in terms of the electron-phonon coupling g_σ , the Raman phonon matrix element T_σ , and the Raman electronic matrix element γ_σ , that is, $S_0 = T_\sigma/(\gamma_\sigma \cdot g_\sigma)$. In our model, g_σ , T_σ , and γ_σ are assumed to be real and therefore S_0 is real. The Kramers-Kronig related functions $R_\sigma(\omega)$ and $\rho_\sigma(\omega)$ denote real and imaginary parts of the electronic response function, respectively, $\chi_\sigma(\omega) = R_\sigma(\omega) + i\rho_\sigma(\omega)$. While the first term in Eq. (1), $\rho_\sigma(\omega)$, describes the “bare” electronic Raman response, the second term represents the phononic contribution and its coupling to the electronic background. We will use expression (1) to describe the coupling of the electronic background to the phonons whose lineshapes exhibit the clearest manifestations of the electron-phonon interaction (e.g., the in-plane B_{1g} phonon). The electronic re-

sponse function $\chi_\sigma(\omega)$ can either be computed from a microscopic model⁴³ or be determined from a fit to the Raman data using a phenomenological model function.^{18,40,41,45} These two approaches will be described in the following two subsections.

It is instructive to note that formula (1) can be brought into the form of the widely used “standard” Fano profile^{17,18,34,46}

$$I_F(\omega) = C_F(q + \epsilon)^2/(1 + \epsilon^2), \quad (2)$$

with the asymmetry parameter

$$q = -S(\omega)/[\rho(\omega)] \quad (3)$$

and $\epsilon = (\omega - \omega_0)/\Gamma$ as in Eq. (1). To extract renormalized phonon parameters the Raman spectra are often fitted using the above Fano profile, Eq. (2), with the Fano parameter q , the intrinsic phonon frequency ω_0 , and the renormalized phonon line width Γ (half-width at half-maximum, HWHM) kept frequency independent. While such an approach can give valuable insights into the temperature dependence of the phonon lineshapes, the *intrinsic* electron-phonon coupling constants and the shape of the electronic continuum $\chi(\omega)$ in the SC state cannot be determined. We will compare the simplified Fano formula (2) with our generalized theory [Eq. (1)] in Sec. IV.

A. Phenomenological model of the electronic response function

To apply the phenomenological model function [Eq. (1)] we need to either assume an expression that describes the real and imaginary parts of the electronic response function $\chi(\omega)$, or compute the electronic Raman response from a microscopic model. Let us first describe a phenomenological model function for $\chi(\omega)$. Following along the lines of Refs. 40,41,45,47 we express the imaginary part of the Raman efficiency with three terms

$$\rho(\omega) = C_n \frac{\omega}{\sqrt{\omega^2 + \omega_T^2}} + \left[\frac{C_1}{1 + \epsilon_1^2(\omega)} - (\omega \rightarrow -\omega) \right] - \left[\frac{C_2}{1 + \epsilon_2^2(\omega)} - (\omega \rightarrow -\omega) \right], \quad (4)$$

where $\epsilon_1(\omega) = (\omega - \omega_1)/\Gamma_1$ and $\epsilon_2(\omega) = (\omega - \omega_2)/\Gamma_2$. The first term in Eq. (4) models an incoherent electronic background, which dominates the response in the normal state of cuprate superconductors. It is linear in ω at small frequencies and becomes constant for large Raman shifts⁴⁴. The second and third terms are Lorentzians describing the pair-breaking peak located below 2Δ , and the suppression of spectral weight at low frequencies, respectively. The latter is due to the opening of the SC gap. To reduce the number of free fitting parameters, we set $\omega_2 = \Gamma_2 = (\omega_1 - \Gamma_1)/2$. The last two terms in Eq. (4) decrease in intensity and shift spectral weight to lower frequency as the superconducting transition temperature T_c is approached from below. ($\omega \rightarrow -\omega$) terms, similar to the C_1 and C_2 terms but with ω replaced by $-\omega$, are essential to achieve the symmetry requirements for the Raman response. In the normal state, the electronic response function is entirely described by the incoherent contribution [first

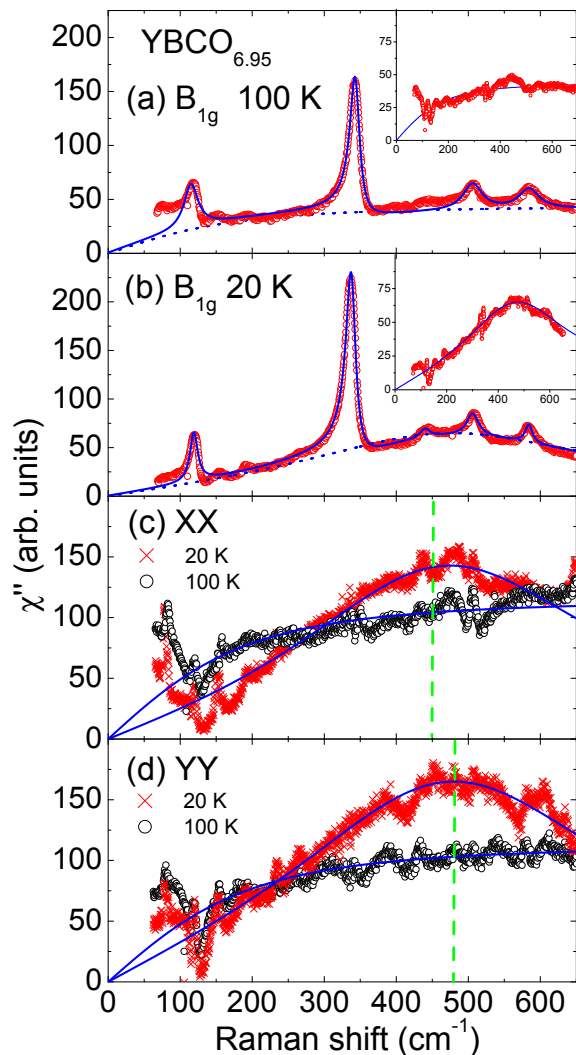


FIG. 2: (color online) B_{1g} Raman spectra of $\text{YBCO}_{6.95}$ ($\lambda = 514.5$ nm) in the normal state at $T = 100$ K (a) and in the superconducting state at $T = 20$ K (b). Open circles show the experimental data, the solid curve the fitting result with formula (1) and four Lorentzians for the remaining A_{1g} phonons. The insets show the corresponding data after phonon subtraction. Panels (c) and (d) show the phonon-subtracted spectra for the xx and yy channels, respectively. The vertical lines indicate the maxima of the electronic peak intensity at 450 cm^{-1} and 480 cm^{-1} , respectively.

term in Eq. (4)]. The real part of the electronic response function, $R(\omega)$, is obtained from the Kramers-Kronig transform of $\rho(\omega)$. Since $R(\omega)$ renormalizes the phonon frequency ω_0 and the parameter S_0 , formula (1) together with Eq. (4) and its Kramers-Kronig transform yield a self-consistent analysis of the Raman spectra. To compute the Kramers-Kronig transform of the incoherent part in Eq. (4), a cut-off frequency ω_c has to be introduced, which results in a constant offset in the real part of the electronic response $R(\omega)$. Provided ω_c is chosen large enough, however, this error only leads to negligibly small corrections.

We have employed a non-linear fit procedure with ten (six)

$\text{YBCO}_{6.95}$	S_0	$2\Gamma_0$	ω_0	$\omega_0(\text{INS})$	$\omega_0(\text{sqrt})$	$\omega_0(\text{lin.})$
B_{1g} (100K)	1.5	15.3	343.1	343.9	342.8	341.9
XX (100K)	1.8	12.2	342.9	343.9	339.1	340.7
YY (100K)	1.8	12.2	342.9	343.9	339.5	338.7
B_{1g} (20K)	2.6	14.8	338.6	338.4	335.8	335.7
XX (20K)	4.1	13.2	336.4	338.4	333.0	332.5
YY (20K)	2.1	13.8	336.3	338.4	334.2	334.2

TABLE I: Extracted parameter values of the B_{1g} oxygen vibration in $\text{YBCO}_{6.95}$ measured at 20 K and 100 K, respectively. Left part: asymmetry parameter S_0 , intrinsic phonon linewidth (FWHM) $2\Gamma_0$, and intrinsic phonon frequency ω_0 using the generalized Fano approach of Eq.(1). Right part: ω_0 extracted with Eq.(2) for different phenomenological electronic backgrounds [sqrt = first term in Eq.(4); lin. = linear background with offset at $\omega = 0$]. For comparison we display in the middle part ω_0 obtained from inelastic neutron scattering (INS) experiments by Reznik *et al.*⁶⁴

independent fit parameters to the Raman spectra of $\text{YBCO}_{6.95}$ and $\text{YBCO}_{6.95:\text{Ca}}$ in the superconducting (normal) state. C_n and ω_T describe the intensity and position of the maximum of the normal-state electronic background given by the square root of a rational function. In the superconducting state C_1/C_2 , $\omega_{1,2}$, and $\Gamma_{1,2}$ describe amplitude, position and width of a Lorentzian function reflecting the region of the pair-breaking peak. Finally, Γ_0 , ω_0 , and S_0 effectively characterize amplitude, width, position, and asymmetry of a generalized Fano function (describing the B_{1g} phonon). Note that for not too strong frequency dependences of $\rho(\omega)$ and $R(\omega)$, the renormalization of the Fano formula due to the electronic background can be simply viewed as an offset of the parameters entering in the Fano formula [cf. Eqs. (1), (2), and (3)]. The results of this fit procedure are shown in Fig. 2 and Fig. 3 together with the experimental data. Table I lists the corresponding fit parameters. Note that on general grounds the extracted ω_0 and Γ_0 parameter values need to be identical at a given temperature for all measurements of a given phonon. In Table I we show, however, the parameter values that correspond to the best (non-linear least squares) fit to the data. The differences reflect the error bars of our procedure. It is important to emphasize that the Fano profile of the B_{1g} -mode shown in Figs. 2, 3 and 4(a) results from the interaction with the electronic Raman signal; *both* electronic and phononic contributions and their interdependence can be described by Eqs. (1) and (4). The final result agrees well with the measured data. Thus, our model allows us to some extent to disentangle the electronic and phononic parts of the Raman response, and to identify the shape of the electronic background. However, strictly speaking, only a combination of parameters such as $g^2\rho$ and g^2R can be extracted. In the next subsection this procedure will be improved for the SC state by employing a microscopic description of the pair-breaking excitations.

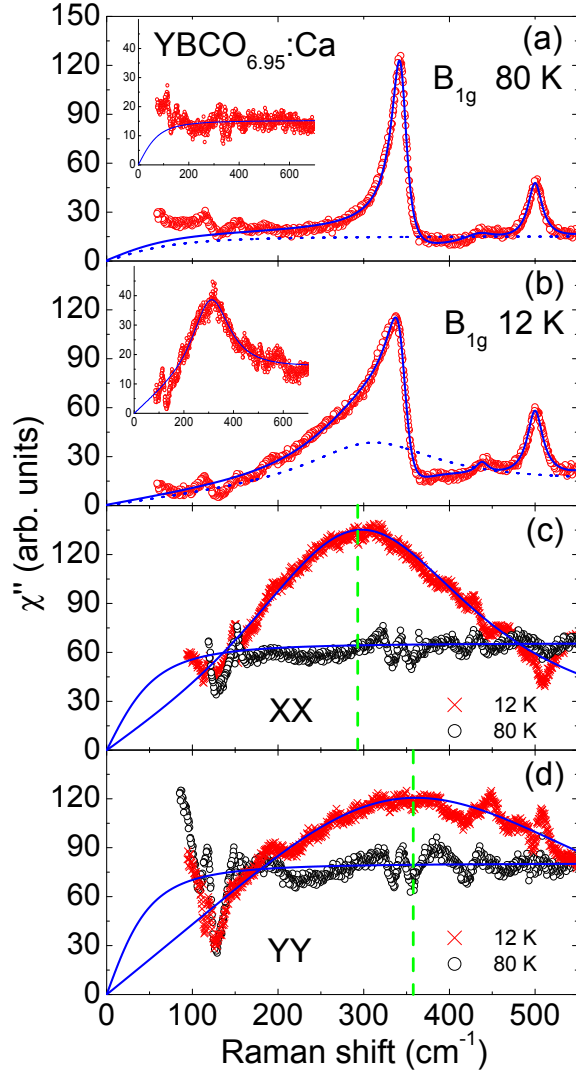


FIG. 3: (color online) Same as Fig. 2 but for the overdoped sample $\text{YBCO}_{6.95}\text{Ca}$. The vertical lines indicate the maxima of the electronic peak intensity at 290 cm^{-1} (XX) and 355 cm^{-1} (YY), respectively.

B. Microscopic description of the superconducting state

To describe the polarization-dependent electronic response function $\chi_\sigma(\omega)$ in the superconducting state, we employ a microscopic model using a realistic tight-binding band structure with anisotropic hopping parameters and a superconducting gap with a mixture of $d_{x^2-y^2}$ - and s -wave symmetries. Such a microscopic approach in conjunction with the analysis of the Raman spectra based on Eq. (1) allows us to obtain precise information about the wavevector dependence of the superconducting order parameter. In particular, we are interested in estimating the magnitude of a possible s -wave admixture to the $d_{x^2-y^2}$ pair wave function.

The starting point of our calculation is the microscopic model introduced in Ref. 21. The electronic Raman response

function in the SC state for a given symmetry channel σ is described by^{16,21,43,48}

$$\chi_\sigma(\omega) = \langle \gamma_\sigma^2 \theta_{\mathbf{k}}(\omega) \rangle - \frac{\langle \gamma_\sigma \theta_{\mathbf{k}}(\omega) \rangle^2}{\langle \theta_{\mathbf{k}}(\omega) \rangle}, \quad (5)$$

$\theta_{\mathbf{k}}(\omega)$ being the Tsuneto function. The angular brackets denote the average over the Brillouin zone, that is,

$$\begin{aligned} \langle (\dots) \theta_{\mathbf{k}}(\omega) \rangle &= \frac{1}{V} \sum_{\mathbf{k}} (\dots) \Delta_{\mathbf{k}}^2 \tanh\left(\frac{E_{\mathbf{k}}}{2T}\right) \\ &\times \left(\frac{1/E_{\mathbf{k}}^2}{\omega + i\eta + 2E_{\mathbf{k}}} - \frac{1/E_{\mathbf{k}}^2}{\omega + i\eta - 2E_{\mathbf{k}}} \right). \end{aligned} \quad (6)$$

The quasiparticle dispersion $E_{\mathbf{k}} = \sqrt{\varepsilon_{\mathbf{k}}^2 + \Delta_{\mathbf{k}}^2}$ contains an effective one-band description of a single copper-oxygen plane

$$\begin{aligned} \varepsilon_{\mathbf{k}} &= -2t [(1 + \delta_0) \cos k_x + (1 - \delta_0) \cos k_y] \\ &\quad - 4t' \cos k_x \cos k_y - \mu, \end{aligned} \quad (7)$$

and the superconducting gap

$$\Delta_{\mathbf{k}} = \frac{\Delta_d}{2} (\cos k_x - \cos k_y) + \Delta_s. \quad (8)$$

For the computation of the electronic Raman response in the superconducting state, Eq. (5), we have assumed the same band structure parameters as in Ref. 21 together with $\Delta_d = 30 \text{ meV}$ and $\Gamma_e = 5 \text{ meV}$.

The Raman vertices γ_σ in Eq. (5) can be classified according to the irreducible representations of the symmetry group of the crystal. Since we shall consider a model with small distortions, $\delta_0 \ll 1$, $\Delta_s \ll \Delta_d$, we use the notation corresponding to tetragonal symmetry, as in Sec. II above. We can thus express, for example, the B_{1g} Raman vertex as

$$\gamma_{B_{1g}, \mathbf{k}} \propto t [(1 + \delta_0) \cos k_x - (1 - \delta_0) \cos k_y] \quad (9)$$

To describe the combined electronic and phononic Raman response in the SC state, we use Eq. (1) together with the real and imaginary parts of the electronic Raman response in the SC state, Eq. (5). Furthermore, we assume that the bare fit parameters do not change as we go from the normal state to the SC state.

In Figure 4(a) we show numerical results obtained from our theoretical model and their comparison with the data on $\text{YBCO}_{6.95}$ obtained in B_{1g} -polarization. The calculations have been performed at $T = 20 \text{ K}$ and for various s -wave contributions. The best description for both the B_{1g} -mode and the electronic response is found if Δ_s is assumed to be 10 percent of the maximum of the $d_{x^2-y^2}$ -wave gap (short dotted line); this also accounts for the slight shift of the pair breaking peaks in xx and yy polarizations (Fig. 2 c and d). Furthermore, our numerical results solely for the electronic response, i.e. the 2Δ -pair-breaking peak, are also displayed in Fig. 4 (dashed, dotted and dash-dotted lines). They are obtained by setting all phononic parts and the corresponding interference terms in Eq. (1) to zero. Interestingly, we find that the pair-breaking peak shifts to lower energies with increasing Δ_s , a

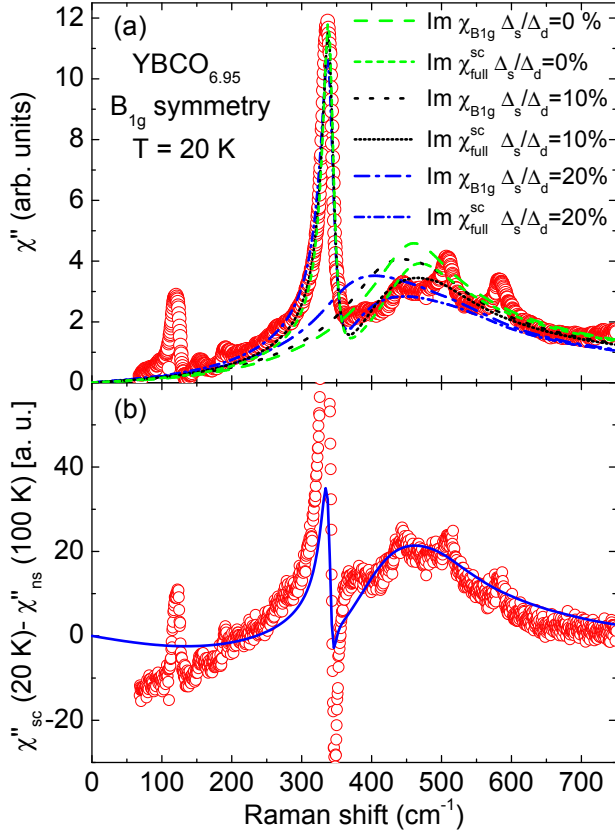


FIG. 4: (color online) (a) B_{1g} Raman spectra of $\text{YBCO}_{6.95}$ in the superconducting state at $T = 20$ K ($\lambda=514.5$ nm). Open circles show the experimental data. The short dashed, short dotted, and short dash-dotted curves are the theoretical result obtained with Eq. (5). The B_{1g} phonon was also taken into account. We show results for various s -wave contributions $\Delta_s/\Delta_d = 0$ (dashed); 0.1 (dotted); 0.2 (dash-dotted). The dashed, dotted, and dash-dotted curves show the calculated imaginary part of the electronic response, $\chi''_{B_{1g}}(\omega)$. (b) Subtracted spectra [20K (sc-state)-100K (n-state)] for the B_{1g} polarization channel of $\text{YBCO}_{6.95}$. Before subtraction the spectra were divided by the Bose factor. The solid curve depicts the theoretical result for 10% s -wave contribution.

fact which has been discussed in a previous paper by Schnyder *et al.*²¹. In addition, the cubic low-energy response, i.e. its $(\omega/2\Delta_0)^3$ -behavior found for $\Delta_s = 0$ changes if $\Delta_s \neq 0$: we obtain linear correction terms which are, however, proportional to Δ_s/Δ_d , and thus barely observable.³

Figure 4(b) shows the differences $(\chi''_S - \chi''_N)$, which were obtained by subtracting the spectra at 20 and 100 K after dividing by the Bose factor. The solid line is obtained after subtracting the model function (4) for the normal state [see Fig. 2(a)] from the results for the SC state when $\Delta_s/\Delta_d = 0.1$ [dotted line in Fig. 4(a)]. We find that the position of the pair-breaking peak at ~ 460 cm^{-1} (and partly its shape) is well described by our theory. This confirms that 10% s -wave contribution [short dotted line in Fig. 4(a)] yields an excellent description of the electronic Raman response. Furthermore,

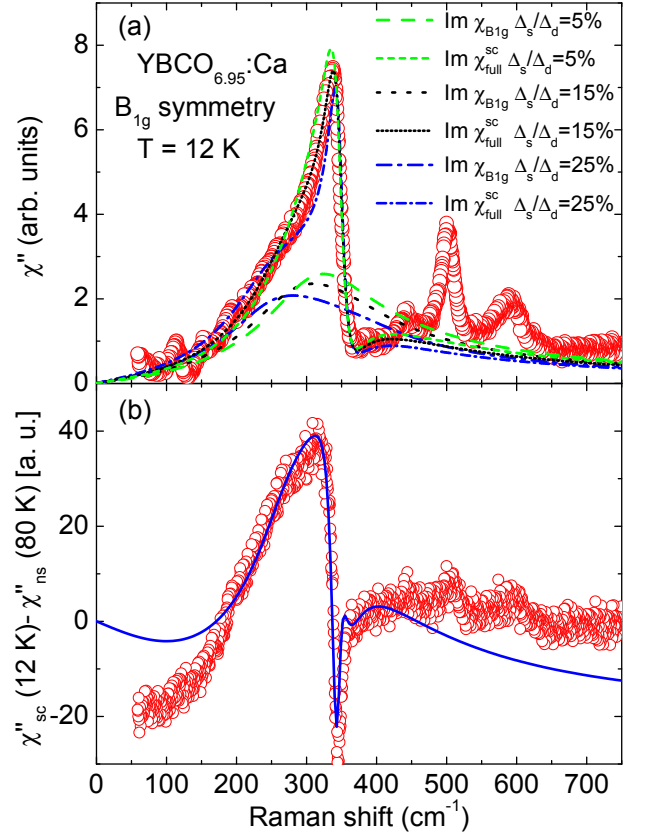


FIG. 5: (color online) (a) B_{1g} Raman spectra of $\text{YBCO}_{6.95}:\text{Ca}$ in the superconducting state at $T = 12$ K ($\lambda=514.5$ nm). Open circles show the experimental data. The short dashed, short dotted, and short dash-dotted curves are the theoretical result obtained with Eq. (5). The B_{1g} phonon was also taken into account. We show results for various s -wave contributions $\Delta_s/\Delta_d = 0.05$ (dashed); 0.15 (dotted); 0.25 (dash-dotted). The dashed, dotted, and dash-dotted curves show the calculated imaginary part of the electronic response, $\chi''_{B_{1g}}(\omega)$. (b) Subtracted spectra [12K (sc-state)-80K (n-state)] for the B_{1g} polarization channel of $\text{YBCO}_{6.95}:\text{Ca}$. Before subtraction the spectra were divided by the Bose factor. The solid curve depicts the theoretical result for 15% s -wave contribution.

the temperature-dependence of the related B_{1g} phonon is also reproduced (see below). Note that the difference between experimental and calculated data at small energies is likely to be due to elastic impurity scattering which is not taken into account in our theoretical model.⁴⁹

Finally, we return to the moderately overdoped sample. Raman data on $\text{YBCO}_{6.95}:\text{Ca}$ above and below T_c in several polarization geometries are displayed in Fig. 3. In the absence of specific information about the electronic band dispersions of this material, we modeled these data by scaling the magnitude of the energy gap Δ_d by the ratio of transition temperatures, keeping all other model parameters identical to those used for $\text{YBCO}_{6.95}$. The best fit was obtained for $\Delta_s/\Delta_d = 0.15$ (however the estimated error bars are about ± 0.05), slightly larger than the corresponding quantity

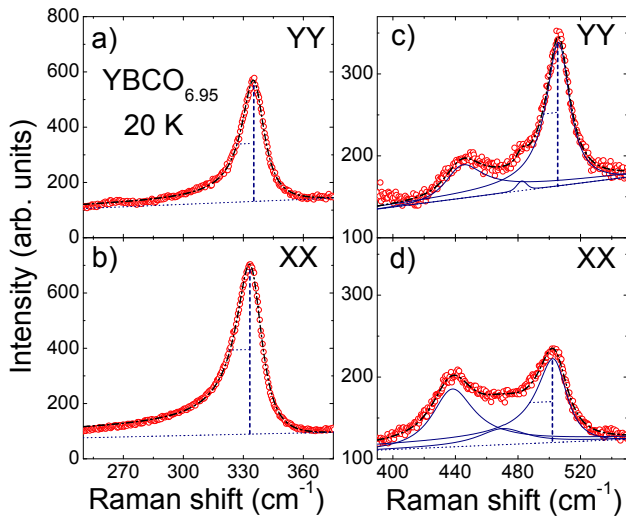


FIG. 6: (color online) Fano-analysis [Eq.(2)] of three different phonons measured at a temperature of 20 K ($\lambda=514.5$ nm). (a,b) The fit of the 340 cm^{-1} mode, which corresponds to the out-of-phase vibrations of the planar oxygen, along yy and xx polarizations, respectively.(c,d) same as (a,b) but for the in-phase planar oxygen mode around 440 cm^{-1} and apical oxygen mode at 501 cm^{-1} . Open circles show the experimental data. The dash-dotted lines are the results of the overall fit to the experimental data. The solid lines are the results of fits to Fano-profiles [Eq.(2)] as described in the text. The dotted lines correspond to a linear background. The intensity units are arbitrary but the same in the four vignettes.

in $\text{YBCO}_{6.95}$. Note that the quality of the fit is comparable to the one for $\text{YBCO}_{6.95}$, although separate plane and chain subsystems were not introduced in the analysis.⁵⁰ The previously observed difference between spectra in xx and yy geometry was confirmed (Fig. 3), but our model calculations suggest that this is a consequence of the s -wave admixture to the gap,³ obviating the need to introduce quantum interference between scattering from chains and planes.^{50,51}

IV. TEMPERATURE DEPENDENT PHONON LINESHAPES

A. Anisotropic Fano profile

Several phonons in YBCO display a pronounced asymmetric lineshape suggesting a strong interaction with the electronic continuum. As shown in Fig. 6 the asymmetry is most pronounced for the 340 cm^{-1} mode. Interestingly, the phonon peak reflecting the vibration of the apical oxygen at 501 cm^{-1} exhibits a strong asymmetry for a polarization of incident and scattered light along the a -axis, whereas along the b -axis the phonon appears to be almost symmetric (see Fig. 6). Two additional modes are present in this spectral range. The mode at 440 cm^{-1} originates from an in-phase vibration of the oxygen atoms O2 and O3. Additional modes are present at about 472 cm^{-1} and 480 cm^{-1} for polarizations parallel to the a - and b -axis, respectively. As mentioned above, these modes

are Raman forbidden, but correspond to IR allowed vibrations involving the Cu1-O1 chains.⁵² Due to defects (oxygen vacancies) in the Cu1-O1 chains they become Raman active.

Similar to previous temperature dependent Raman experiments on $\text{YBCO}_{7-\delta}$ ^{33,53} and $\text{HgBa}_2\text{Ca}_3\text{Cu}_4\text{O}_{10+\delta}$,⁵⁴ we have fitted the phonons of $\text{YBCO}_{6.95}$ by using simple Fano profiles. The solid lines in Fig. 6 are the results of fits to the experimental data using Eq. (2), the dash dotted lines correspond to the resulting fitted lineshape of the entire spectrum. The calculated profiles agree well with the measured spectra. In order to obtain estimates of the intrinsic phonon positions and linewidths, we have corrected the peak position and linewidth by the procedure used in Ref. 20. We find for the xx -symmetry, i.e., polarizations along the a -axis:

$$\omega_{xx} = \omega_0 + \Gamma/q_{xx} \quad \text{and} \quad \Gamma_{\text{FWHM}}^{xx} = 2\Gamma \left| \frac{(1 + q_{xx}^2)}{(1 - q_{xx}^2)} \right| \quad (10)$$

$\Gamma_{\text{FWHM}}^{xx}$ denotes the intrinsic full width at half maximum (FWHM)⁵⁵. For the yy -polarizations one obtains an analogous equation.

Fits to the simplified Fano profile of Eq. (2) are much less complicated than the fitting procedure to the full spectrum discussed above. This is a key advantage especially in situations in which several closely spaced phonons partially overlap as is the case, for instance, for the apical-oxygen vibration in Fig. 6. The multi-parameter, global fit [Eq. (1)] yields unstable results for these phonons. It is important to note, however, that the quantities extracted from simple Fano fits are renormalized by the electronic response function, and therefore deviate slightly from the intrinsic phonon frequency ω_0 and the bare linewidth Γ_0 of Table I. We will compare the results of both procedures in detail at the end of the next subsection.

B. Superconductivity-induced changes in the position and linewidth

Figure 7 shows the temperature dependence of the energies and linewidths of two particular phonons, the 340 cm^{-1} and 501 cm^{-1} modes, measured with light polarization along the crystallographic a - and b -axes. The spectra were taken at temperatures ranging from 20 to 300 K. The temperature dependence of the phonon energy and linewidth in the normal state arises from anharmonic phonon-phonon interactions, i. e., the decay of a high-energy optical phonon into two phonons of lower energy with opposite momenta^{56,57}. For simplicity, assuming the resulting phonons to have the same energy^{56,57} and using Bose-Einstein statistics, this decay process leads to $\Gamma_{anh.}(T) = \Gamma_{anh.}^{T=0}(1 + 2n(\omega_p/2))$. This process, implying decay through real transitions, is strictly valid for the line width, but has been also used for the frequency shift although, in this case, virtual transitions also play a role. In Fig. 7, both linewidth and peak position were fitted simultaneously for the temperature range above T_c (solid lines). Both of these quantities show abrupt changes at the SC transition temperature due to the opening of the superconducting gap, as previously observed in YBCO (see for example

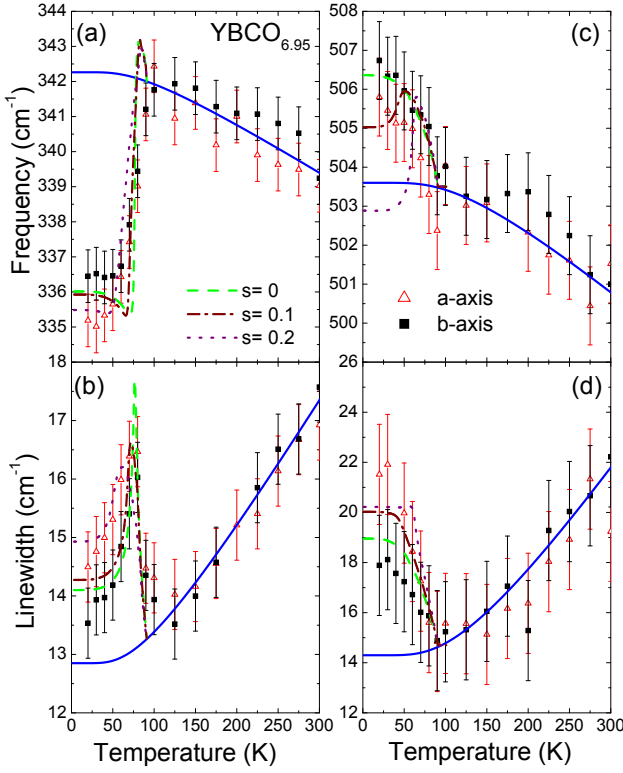


FIG. 7: (color online) Frequency and line width (FWHM) obtained using Eqs. (2) and (10) versus temperature of the 340 cm^{-1} mode and the 501 cm^{-1} mode of $\text{YBCO}_{6.95}$ for the xx - and yy -polarization, respectively ($\lambda=514.5\text{ nm}$). Below T_c a comparison between calculations for $s = \Delta_s/\Delta_d = 0$ (dashed line), 0.1 (dash-dotted line), and 0.2 (dotted line) is displayed. The solid line corresponds to the temperature dependence of pure phonon-phonon interaction (interpreted as Klemens decay into two phonons of equal frequencies).

Refs. 33,53) and also other superconducting compounds like $\text{HgBa}_2\text{Ca}_3\text{Cu}_4\text{O}_{10}$ ⁵⁴ and $\text{Bi}_2\text{Sr}_2\text{CaCu}_2\text{O}_8$.^{58,59}

Within the error bars of $\sim 0.8\text{ cm}^{-1}$ in (a)-(c) and 2.0 cm^{-1} in (d), the phonon peak position and linewidth of the 340 cm^{-1} mode is the same for the xx and yy polarizations (see Fig. 7a and b). Taking the phonon positions and linewidths in the SC state as ω_p^s and Γ_p^s , the maximum change in the phonon position and linewidth is obtained from $\Delta\omega = \omega_p^s(T) - \omega_p(T = 100\text{ K})$ and $\Delta\Gamma = \Gamma_p^s(\tilde{T}) - \Gamma_p(T = 100\text{ K})$,⁶⁰ where \tilde{T} denotes the temperature at which the maximum of the SC-induced changes occurs. The additional softening below T_c due to the electron-phonon interaction is about -6 cm^{-1} . The change in linewidth (FWHM) is $+3\text{ cm}^{-1}$, reflecting a broadening. For the vibration of the apical oxygen, i.e. the 501 cm^{-1} mode, the corresponding shift and broadening are $+3\text{ cm}^{-1}$ and $+5\text{ cm}^{-1}$, respectively. The SC-induced changes for the 340 cm^{-1} and 501 cm^{-1} modes are in good agreement with previous data obtained on twinned YBCO .^{33,53,60}

The SC-induced changes in the phonon linewidth and peak position (for a phonon labeled as μ) can be related to changes in the phonon self-energy $\Sigma_\mu(\omega) = |g^\mu|^2 \Pi(\omega + i\eta)$ (with

$\eta \rightarrow 0$), resulting from the interaction between the phonons and the electronic system below T_c .^{21,48,59} The induced frequency shifts $\Delta\omega$ are related to the real part of the phonon polarization Π by^{48,61,62}

$$\frac{\Delta\omega}{\omega} = \frac{1}{N(0)} \lambda \text{Re}\Pi, \quad (11)$$

while the induced changes in the linewidth can be calculated via

$$\frac{\Delta\Gamma}{\omega} = \frac{1}{N(0)} \lambda \text{Im}\Pi. \quad (12)$$

Here, $N(0)$ denotes the electronic density of states at the Fermi level and $\lambda = 2 \sum_{\mathbf{k}} \sum_{\mu} \int \frac{d\omega}{\omega} |g_{\mathbf{k},0}^\mu|^2 F_{\mathbf{k}}^\mu(\omega) \delta(\epsilon_{\mathbf{k}})$ is the dimensionless electron-phonon coupling constant. $F_{\mathbf{k}}^\mu(\omega)$ denotes the spectral function for phonon μ under consideration.⁶³ Taking into account screening effects, i.e. the long-range Coulomb force, the self-energy is given by:^{21,48,61,62}

$$\Sigma_\lambda(\omega) = - \left\langle \left(g_{\mathbf{k},0}^\mu \right)^2 \theta_{\mathbf{k}}(\omega) \right\rangle + \frac{\left\langle g_{\mathbf{k},0}^\mu \theta_{\mathbf{k}}(\omega) \right\rangle^2}{\langle \theta_{\mathbf{k}}(\omega) \rangle}, \quad (13)$$

where the angular brackets are defined by Eq. (6). The symmetry of the optical phonons is reflected in the matrix element $g_{\mathbf{k},0}^\mu$. The electron-phonon coupling of phonons of A_{1g} and B_{1g} symmetry are in a first approximation given by

$$\begin{aligned} g_{\mathbf{k},0}^{B_{1g}} &= g_{B_{1g}} (\cos k_x - \cos k_y)/2, \\ g_{\mathbf{k},0}^{A_{1g}} &= g_{A_{1g}} (\cos k_x + \cos k_y)/2. \end{aligned} \quad (14)$$

with the electron-phonon coupling strength $g_{B_{1g}}$ and $g_{A_{1g}}$ (Note that there is more than one phonon of A_{1g} symmetry). In general, the phonons below the energy of the superconducting gap $2\Delta_{max}$ should soften below T_c (i.e. they should shift to lower energies), whereas phonons above $2\Delta_{max}$ should harden. This is confirmed in our experiments (not all data are shown here) and in previous work (see Refs. 19, 33, and 53). The energy of the apical oxygen phonon ($501\text{ cm}^{-1} = 62.5\text{ meV}$) is right at the gap energy and is therefore sensitive to small changes in the energy of the SC gap. The 340 cm^{-1} mode is well below the SC energy gap for $T \ll T_c$. With increasing temperature the energy of the 2Δ gap shifts to lower energies and moves through the energy of the 340 cm^{-1} mode. This explains the maximum of the linewidth at 75 K . A similar behavior was observed by Limonov *et al.*¹⁸.

Finally, we discuss the role of the s -wave contribution to the superconducting gap which has been introduced in Eq. (8). Our numerical results obtained with Eqs. (5)–(8) and Eqs. (11)–(14) using the fits reported in Sec. III are also displayed in Fig. 7. We compare $\Delta_s = 0$ (dashed line) with $\Delta_s = 3\text{ meV}$ (dash-dotted line) and $\Delta_s = 6\text{ meV}$ (dotted line). We find that the results obtained with 20 percent s -wave contribution cannot describe our data. This is clearly visible in Figs. 7(a) and (c) which show the SC-induced changes $\Delta\omega$ in the position of the corresponding phonon. In particular, for

the 501 cm^{-1} -mode which is known to be very sensitive to the superconducting gap,²¹ one predicts a softening for $\Delta_s = 6$ meV, while instead a hardening is observed. Therefore, our data imply an upper limit of $\Delta_s/\Delta_d = 0.2$. The best agreement is obtained for 10% s-wave admixture.

At the end of this subsection, we are contrasting our generalized Fano theory [see Eq. (1)] with the standard Fano approach described by Eqs. (2) and (10). The main difference between both approaches is the theoretical description of the electronic Raman response. While in the standard Fano approach the background is assumed either to be linear (see Fig. 6) or to follow a square-root behavior⁶⁸ [first term in Eq. (4)] in both the normal and SC-state, our generalized Fano theory is able to take the rearrangement of spectral weight due to the opening of the superconducting gap into account. Within our microscopic description [Eqs. (5)–(8)] it is then possible to determine the ratio Δ_s/Δ_d . Another difference between both Fano theories concerns the asymmetry parameter q : in our generalized theory it becomes ω -dependent which allows a self-consistent description of the B_{1g} -phonon and the electronic Raman response from 80 to about 1000 cm^{-1} . Thus, in other words, no specific frequency interval close to the phonon peak position [see Fano lineshape analysis in Figs. 6(a) and (b)] needs to be selected.

We have summarized our comparison in Table I in which the intrinsic frequency of the B_{1g} -phonon extracted from both Fano theories is displayed: ω_0 obtained from Eq. (1) [left part, third column], ω_0 obtained from Eqs. (2) and (10) either for a square-root [$\omega_0(\text{sqrt})$] or linear background [$\omega_0(\text{lin.})$] (right part). These values have to be compared with ω_0 obtained from inelastic neutron scattering experiments [$\omega_0(\text{INS})$] (middle column). One clearly sees that the values for ω_0 obtained from our generalized Fano theory are similar to those measured in INS experiments. On the other hand, the values extracted from the standard Fano approach differ by 1.1 [B_{1g}(100K), $\omega_0(\text{sqrt})$] to 5.9 [XX(20K), $\omega_0(\text{lin.})$] wavenumbers. Note, however, that these values can be substantially modified if a specific frequency interval around the peak position of the B_{1g} -phonon is defined and the corresponding lineshape analysis is then restricted to this interval (see Fig. 6.) These improved values are shown in Fig. 7. In the case of the apical oxygen vibration analyzed in Figs. 6(c) and (d), a fit with Eq. (1) is hardly possible due to the multiple peak structure between 400 cm^{-1} and 540 cm^{-1} . Therefore, we have used Eqs. (2), (4), and (10). On the whole, we find characteristic differences between our self-consistent, generalized Fano theory and the standard Fano approach, but our conclusions about the ratio Δ_s/Δ_d are independent of the theory used provided that Eqs. (2), (4), and (10) are restricted (or strongly weighted) to an interval around the peak position of the phonon being investigated.

C. Temperature dependence of the asymmetry parameter

Figure 8 shows the temperature dependence of the asymmetry parameters q_{xx}^{-1} and q_{yy}^{-1} in Eq. (2) as obtained from the fits of the Fano profile to the experimental spectra. We discuss

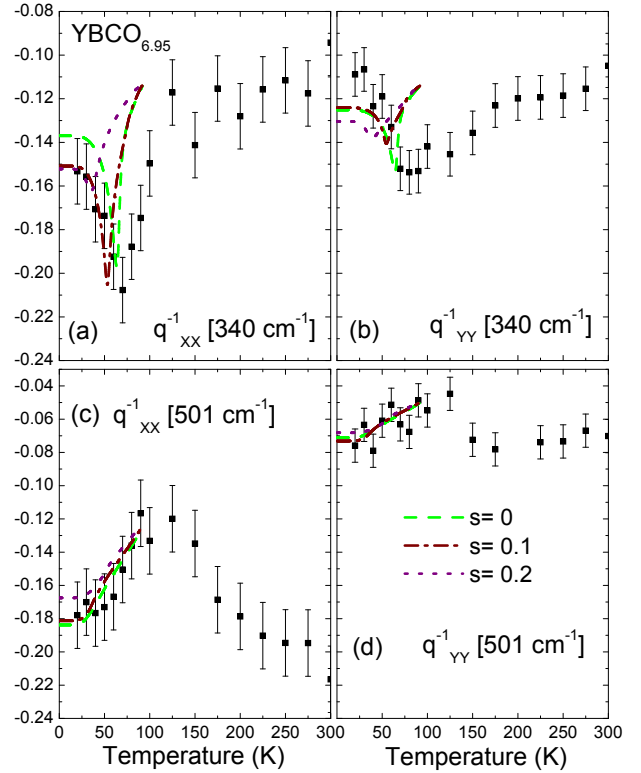


FIG. 8: (color online) Fano asymmetry parameter ($\lambda = 514.5\text{ nm}$) of both polarization channels for the 340 cm^{-1} and 503 cm^{-1} mode of $\text{YBCO}_{6.95}$, respectively. Results of the theoretical calculations for different s-wave admixtures (0, 0.1, and 0.2) are also shown.

these data in the framework of the approximate expression

$$q \approx \frac{T_\sigma/\gamma_\sigma}{g_\sigma \chi''_\sigma}, \quad (15)$$

already applied in Raman work on other high T_c superconductors.^{37,54,65} We first focus on temperatures above T_c and note that $q_{xx}^{-1} \approx q_{yy}^{-1} \sim -0.12$ for the 340 cm^{-1} mode, whereas a pronounced difference in the asymmetry parameters along in xx and yy geometries is observed for the 501 cm^{-1} mode ($q_{xx}^{-1} \sim -0.20$, $q_{yy}^{-1} \sim -0.08$). As g_σ is a materials parameter independent of the light-field configuration and χ''_σ is weakly ω -dependent, the strong variation of asymmetry parameters must be attributed to differences in T_σ/γ_σ . Our results are in fair agreement with the phononic and electronic Raman efficiencies (proportional to $|T_\sigma|^2$ and $|\gamma_\sigma|^2$, respectively) calculated in refs. 66,67 using density functional methods. For instance, the calculated $\frac{|\gamma/T|_{yy}}{|\gamma/T|_{xx}} (\sim \frac{q_{yy}^{-1}}{q_{xx}^{-1}})$ in the normal state is about 1.2 and 0.65 for the 340 cm^{-1} and 501 cm^{-1} modes, respectively. The changes of the asymmetry parameters with temperature in the normal state may reflect a temperature dependence of γ_σ , *i.e.* parameters in the electronic band structure as well as that of the anharmonic linewidth, but their detailed origin cannot be disentangled

Moving to the superconducting state, we note that the only parameter in Eq. (15) expected to change significantly across

T_c is the response function χ''_{σ} . The temperature dependence of q_{xx}^{-1} and q_{yy}^{-1} below T_c therefore also reflects the *ab*-anisotropy in the 2Δ -gap. Thus we have computed the temperature evolution of the asymmetry parameters in the superconducting state, using the same model parameters described in Sec. III. The reasonable agreement with the data (Fig. 8) demonstrates the self-consistency of our approach. However, since the superconductivity-induced modification of q_{xx}^{-1} and q_{yy}^{-1} is relatively subtle (compared to that observed in the normal state), this analysis does not provide constraints on the ratio Δ_s/Δ_d beyond those already discussed above.

It is interesting to note that other A_g modes also reveal a temperature-dependent asymmetry. In particular, we have observed that the Ba mode near 115 cm^{-1} is symmetric (*i.e.* $q^{-1} = 0$) for $T \rightarrow 0$ and its asymmetry increases monotonically to $q^{-1} = 0.25$ (not shown). Its intensity, however, is rather weak compared with the B_{1g} mode (and this applies even more so to the Cu mode near 150 cm^{-1}), so we have not used these modes further in our discussion. Their asymmetry has been analyzed in more detail in Ref. 69, however without considering a possible *s*-component to the $d_{x^2-y^2}$ -wave gap.

V. SUMMARY AND CONCLUSIONS

In this work we have revisited the superconductivity-induced effects on phononic and electronic Raman scattering in detwinned slightly overdoped $\text{YBa}_2\text{Cu}_3\text{O}_{6.95}$ and moderately overdoped $\text{Y}_{0.85}\text{Ca}_{0.15}\text{Ba}_2\text{Cu}_3\text{O}_{6.95}$ single crystals, both from an experimental and a theoretical point of view. In particular, we have performed a detailed study of the in-plane anisotropies in the electronic continuum and in the phonon

lineshapes and assessed their implications for an *s*-wave admixture to the *d*-wave superconducting gap. To this end, we developed and applied a formalism that treats the frequency dependence of both electronic and phononic Raman scattering on equal footing. Thus we can disentangle both parts and clarify the role of interference terms. Due to this procedure we are able to extract the intrinsic frequency ω_0 of the phonon position reflecting the intrinsic electron-phonon interaction. A comparison shows that ω_0 agrees well with INS data at the Γ -point. The best agreement with the Raman data was obtained by model calculations based on admixtures of 10% and $15\% \pm 5\%$ *s*-wave contribution for $\text{YBa}_2\text{Cu}_3\text{O}_{6.95}$ and $\text{Y}_{0.85}\text{Ca}_{0.15}\text{Ba}_2\text{Cu}_3\text{O}_{6.95}$, respectively. This agrees with values obtained by other experimental methods^{3,4,5,6,7,8} and confirms the previously observed trend⁴ of an increase in the *s*-wave contribution with increasing doping level. Our data do not show evidence of the previously reported⁵⁰ unusual quantum interference between electronic Raman scattering from planes and chains in overdoped $\text{Y}_{1-x}\text{Ca}_x\text{Ba}_2\text{Cu}_3\text{O}_{7-\delta}$.

Acknowledgments

We would like to thank R. Zeyher and J. Unterhinninghofen for helpful discussions and K. Syassen for a critical reading of the manuscript. M.B. thanks V. Hinkov, R. Merkle, and B. Baum for their help in sample preparation and A. Schulz and H. Uhlig for technical support. This work was partially supported by the International Max Planck Research School for Advanced Materials (IMPRS). A. S. thanks the Swiss NSF for its financial support and the Max Planck Institute for hospitality.

-
- ¹ D.A. Wollman, D.J. Van Harlingen, W.C. Lee, D.M. Ginsberg, and A.J. Leggett, Phys. Rev. Lett. **71**, 2134 (1993).
- ² C.C. Tsuei, J.R. Kirtley, C.C. Chi, Lock See Yu-Jahnes, A. Gupta, T. Shaw, J.Z. Sun, and M.B. Ketchen, Phys. Rev. Lett. **73**, 593 (1994); C. C. Tsuei, J. R. Kirtley, Z. F. Ren, J. H. Wang, H. Raffy, Z. Z. Li, Nature **387**, 481 (1997).
- ³ T. Strohm and M. Cardona, Solid State Comm. **104**, 233 (1997); T. Strohm, Ph.D. thesis, University of Stuttgart (1999).
- ⁴ T. Masui, M. Limonov, H. Uchiyama, S. Lee, S. Tajima, and A. Yamanaka, Phys. Rev. B **68**, 060506(R) (2003).
- ⁵ T. Hiramachi, T. Masui, S. Tajima, Physica C, **463**, 89 (2007).
- ⁶ R. Nemetschek, R. Hackl, M. Opel, R. Philipp, M.T. Béal-Monod, J.B. Bieri, K. Maki, A. Erb, and E. Walker, Eur. Phys. J. B **5**, 495 (1998).
- ⁷ D.H. Lu, D.L. Feng, N.P. Armitage, K.M. Shen, A. Damascelli, C. Kim, F. Ronning, Z.-X. Shen, D.A. Bonn, R. Liang, W.N. Hardy, A.I. Rykov, and S. Tajima, Phys. Rev. Lett. **86**, 4370 (2001); H. Uchiyama, T. Masui and S. Tajima, J. Low Temp. Phys. **131**, 287 (2003).
- ⁸ See J.R. Kirtley, C.C. Tsuei, A. Ariando, C.J.M. Verwijs, S. Harkema, and H. Hilgenkamp, Nat. Phys. **2**, 190 (2006), and references therein.
- ⁹ V.B. Zabolotnyy, S.V. Borisenko, A.A. Kordyuk, J. Geck, D.S. Inosov, A. Koitzsch, J. Fink, M. Knupfer, B. Büchner, S.-L. Drechsler, H. Berger, A. Erb, M. Lambacher, L. Patthey, V. Hinkov, and B. Keimer, Phys. Rev. B **76**, 064519 (2007).
- ¹⁰ I. Eremin and D. Manske, Phys. Rev. Lett. **94**, 067006 (2005).
- ¹¹ A. P. Schnyder, D. Manske, C. Mudry, and M. Sigrist, Phys. Rev. B **73**, 224523 (2006).
- ¹² H.A. Mook, P. Dai, F. Dogan, and R.D. Hunt, Nature **404**, 729 (2000).
- ¹³ V. Hinkov, S. Pailhès, P. Bourges, Y. Sidis, A. Ivanov, A. Kulakov, C.T. Lin, D.P. Chen, C. Bernhard, and B. Keimer, Nature **430**, 650 (2004).
- ¹⁴ G. S. Uhrig, K. P. Schmidt, and M. Grüninger, Phys. Rev. Lett. **93**, 267003 (2004).
- ¹⁵ M. Vojta, Th. Vojta, and R. K. Kaul, Phys. Rev. Lett. **97**, 097001 (2006).
- ¹⁶ For a review, see T.P. Devereaux and R. Hackl, Rev. Mod. Phys. **79**, 175 (2007).
- ¹⁷ C. Thomsen, in *Light Scattering in Solids VI*, edited by M. Cardona and G. Güntherodt, Springer Verlag Berlin (1991), p.285.
- ¹⁸ M. F. Limonov, A. I. Rykov, S. Tajima, and A. Yamanaka, Phys. Rev. B **61**, 12412 (2000).
- ¹⁹ M.F. Limonov, A.I. Rykov, S. Tajima, and A. Yamanaka, Phys. Rev. Lett. **80**, 825 (1998).
- ²⁰ T. Strohm, V.I. Belitsky, V.G. Hadjiev, and M. Cardona, Phys. Rev. Lett. **81**, 2180 (1998).

- ²¹ A.P. Schnyder, C. Mudry, and D. Manske, Phys. Rev. B **75**, 174525 (2007).
- ²² E. Faulques, V. G. Ivanov, C. Mézière, and P. Batail, Phys. Rev. B **62**, R9291 (2000).
- ²³ C. T. Lin, B. Liang, H. C. Chen, J. Cryst. Growth **237 - 239**, 778 (2002).
- ²⁴ J. L. Tallon, C. Bernhard, H. Shaked, R. L. Hitterman, and J. D. Jorgensen, Phys. Rev. B **51**, 12911 (1995).
- ²⁵ V.I. Voronkova and Th. Wolf, Physica C **218**, 175 (1993).
- ²⁶ C. T. Lin and A. Kulakov, Physica C **408-410**, 27 (2004).
- ²⁷ F. Slakey, S. L. Cooper, M. V. Klein, J. P. Rice, and D. M. Ginsberg, Phys. Rev. B **39**, 2781 (1989).
- ²⁸ K. C. Hewitt and J. C. Irwin, Phys. Rev. B **66**, 054516 (2002).
- ²⁹ X. K. Chen, J. C. Irwin, H. J. Trodahl, M. Okuya, T. Kimura, K. Kishio, Physica C **295**, 80 (1998).
- ³⁰ X. K. Chen, J. C. Irwin, R. Liang, W. N. Hardy, Physica C **227**, 113 (1994).
- ³¹ M. Le Tacon, A. Sacuto, A. Georges, G. Kotliar, Y. Gallais, D. Colson, A. Forget, Nat. Phys. **2**, 537 (2006).
- ³² M. Cardona, Physica C **317-318**, 30 (1999).
- ³³ C. Thomsen, M. Cardona, B. Gegenheimer, R. Liu, and A. Simon, Phys. Rev. B **37**, 9860 (1988); B. Friedl, C. Thomsen, and M. Cardona, Phys. Rev. Lett. **65**, 915 (1990).
- ³⁴ C. Thomsen and M. Cardona in *Physical properties of high temperature superconductors I*, ed. by D.M. Ginsberg (World Scientific, Singapore, 1988), p.411.
- ³⁵ D.R. Wake, F. Slakey, M.V. Klein, J.P. Rice, and D.M. Ginsberg, Phys. Rev. Lett. **67**, 3728 (1991).
- ³⁶ C. Thomsen and G. Kaczmarczyk in *Handbook of vibrational spectroscopy*, ed. by J. M. Chalmers & P. R. Griffiths (Wiley, Chichester, 2002), pp. 2651-2669.
- ³⁷ M. N. Iliev, V. G. Hadjiev, S. Jandl, D. Le Boeuf, V. N. Popov, D. Bonn, R. Liang, W. N. Hardy, Phys. Rev. B **77**, 174302 (2008).
- ³⁸ A. G. Panfilov, M. F. Limonov, A. I. Rykov, S. Tajima, and A. Yamanaka, Phys. Rev. B **57**, R5634 (1998).
- ³⁹ S. Bahrs, S. Reich, A. Zwick, A. R. Goñi, W. Bacsa, G. Nieve, and C. Thomsen, phys. stat. sol. b **241**, R63 (2004).
- ⁴⁰ A. Bock, S. Ostertun, R. Das Sharma, M. Rübhausen, K.-O. Subke, and C. T. Rieck, Phys. Rev. B **60**, 3532 (1999).
- ⁴¹ A. Bock, Ann. Phys. (Leipzig) **8**, 441 (1999).
- ⁴² X. K. Chen, E. Altendorf, J. C. Irwin, R. Liang, and W. N. Hardy, Phys. Rev. B **48**, 10530 (1993).
- ⁴³ T. P. Devereaux, A. Virosztek, A. Zawadowski, Phys. Rev. B **51**, 505 (1995).
- ⁴⁴ M. Le Tacon, A. Sacuto, Y. Gallais, D. Colson, and A. Forget, Phys. Rev. B **76**, 144505 (2007).
- ⁴⁵ M. Limonov, D. Shantsev, S. Tajima, and A. Yamanaka, Phys. Rev. B **65**, 024515 (2001).
- ⁴⁶ M. V. Klein, in *Light Scattering in Solids I*, edited by M. Cardona, Springer Verlag Berlin (1983), p. 169.
- ⁴⁷ M. Limonov, D. Shantsev, S. Tajima, and A. Yamanaka, Physica C **357-360**, 265 (2001).
- ⁴⁸ T.P. Devereaux, Phys. Rev. B **50**, 10287 (1994).
- ⁴⁹ We emphasize that the low-energy power laws in Figs. 2 and Fig. 4(a) are changed in the presence of an *s*-wave contribution while there exists no power law for the subtracted data in Fig. 4(b).
- ⁵⁰ T. Masui, M. Limonov, H. Uchiyama, S. Tajima, and A. Yamanaka, Phys. Rev. Lett. **95**, 207001 (2005); M. Limonov, T. Masui, H. Uchiyama, S. Lee, S. Tajima, and A. Yamanaka, Physica C **392-396**, 53 (2003).
- ⁵¹ T. Masui, T. Hiramachi, K. Nagasao, and S. Tajima, Phys. Rev. **79**, 014511 (2009).
- ⁵² C. Bernhard, T. Holden, J. Humlicek, D. Munzar, A. Golnik, M. Kläser, Th. Wolf, L. Carr, C. Homes, B. Keimer, and M. Cardona, Solid State Commun. **121**, 93 (2002).
- ⁵³ E. Altendorf, X.K. Chen, J.C. Irwin, R. Liang, and W.N. Hardy, Phys. Rev. B **47**, 8140 (1993); E. Altendorf, J. Chrzanowski, J. C. Irwin, A. O'Reilly, and W. N. Hardy, Physica C **175**, 47 (1991).
- ⁵⁴ V.G. Hadjiev, Xingjiang Zhou, T. Strohm, M. Cardona, Q.M. Lin, and C.W. Chu, Phys. Rev. B **58**, 1043 (1998).
- ⁵⁵ Note that the derivation of Eq. (10) assumes that the Raman intensity $I(\omega)$ can be described by Eq. (2) and an ω -independent background. On the other hand, if $I(\omega) = \frac{(q+\epsilon)^2}{1+\epsilon^2} + \alpha\omega + \beta$ (with $\alpha \neq 0$) is assumed, one obtains higher correction terms for $q > 1$: $\omega_{xx} - \omega_0 = \Gamma/q_{xx} + \frac{1}{2} \frac{1+q_{xx}^2}{q_{xx}^4} \Gamma^2 \alpha + \dots$. Since, however, the slope α is relatively small, those higher corrections are of the order of 2% for the B_{1g} -phonon, for example. Therefore, it is reasonable to work with Eq. (10).
- ⁵⁶ P. G. Klemens, Phys. Rev. **148**, 845 (1966).
- ⁵⁷ J. Menéndez and M. Cardona, Phys. Rev. B **29**, 2051 (1984).
- ⁵⁸ M. Limonov, S. Lee, S. Tajima, and A. Yamanaka, Phys. Rev. B **66**, 054509 (2002).
- ⁵⁹ A.A. Martin, J.A. Sanjurjo, K.C. Hewitt, X.Z. Wang, J.C. Irwin, and M.J.G. Lee, Phys. Rev. B **56**, 8426 (1997).
- ⁶⁰ K. C. Hewitt, X. K. Chen, C. Roch, J. Chrzanowski, J. C. Irwin, E. H. Altendorf, R. Liang, D. Bonn, and W. N. Hardy, Phys. Rev. B **69**, 064514 (2004).
- ⁶¹ R. Zeyher and G. Zwicknagl, Z. Phys. B **78**, 175 (1990).
- ⁶² E. J. Nicol, C. Jiang, and J. P. Carbotte, Phys. Rev. B **47**, 8131 (1993).
- ⁶³ G. D. Mahan, *Many-Particle Physics*, Plenum Press, New York (1981).
- ⁶⁴ D. Reznik, B. Keimer, F. Dogan, and I. A. Aksay, Phys. Rev. Lett. **75**, 2396 (1995).
- ⁶⁵ E. T. Heyen, M. Cardona, J. Karpinski, E. Kaldis, and S. Rusiecki, Phys. Rev. B **43**, 12958 (1991).
- ⁶⁶ E.T. Heyen, Ph.D. Thesis, University of Stuttgart, Germany (1991).
- ⁶⁷ M. C. Krantz, I. I. Mazin, D. H. Leach, W. Y. Lee, and M. Cardona, Phys. Rev. B **51**, 5949 (1995).
- ⁶⁸ This is similar to a $\tanh(\omega/4T)$ -behavior of the electronic background assumed in Ref.41.
- ⁶⁹ E. Faulques and V. G. Ivanov, Phys. Rev. B **55**, 3974 (1997).